Research Journal of Applied Sciences, Engineering and Technology 4(21): 4535-4545, 2012
ISSN: 2040-7467

Submitted: June 08, 2012 Accepted: July 04, 2012 Published: November 01, 2012

A New Skin Detection Approach for Adult Image Identification

A. Nadian Ghomsheh and A. Talebpour
Department of Electronic and Computer Engineering, Shahid Beheshti University, GC, Tehran, Iran

Abstract: With rapid proliferation of adult content on the internet, development of software to detect and filter this content is gaining more and more attention. In this study, a new method for adult image identification is proposed. Accurate human skin detection and extraction of relative features are the bottlenecks in this regard. In the proposed skin detection method, first, Hue color information is utilized to examine whether skin is present in the image, and if so, using dynamic thresholding an estimate of the skin region is obtained. In the second step, for images that contain skin, an exponential function is fitted to the histogram of the estimated skin area. Based on the parameters of the fitted function, the final skin map of the image is extracted. Area, texture, and a new shape feature are extracted from each region and used for image classification using neural networks. 95% accuracy for skin detection and 93.7% accuracy of adult image detection, compared to other methods showed the significance of the proposed method.

Keywords: Dichromatic reflection model, HSV color space, skin detection, objectionable image filtering

INTRODUCTION

Many internet users are potential victims of unwanted pornographic. But the problem becomes more concerning when knowing that 25% of children who gain access to the internet have viewed such content (Wai and Paul, 2004; D'Orlando, 2011). Over-blocking of normal web pages as a result of misclassification is a big problem when filtering is applied and reducing the error rate is crucial (Kranich, 2004).

Two approaches are incorporated in order to decide on the content of web pages. The first method, applied in European countries, uses black lists, updated manually based on human intelligence (Stol, *et al*., 2009). This method is not very efficient since it needs continuing human efforts to keep the list up to date. The second approach uses Dynamic filtering to solve these objections, where textual and visual feature are checked for potential data that needs to be filtered (Haselton, 2007). If textual features are used, a number of keywords are extracted from the web page, and if the frequency and plurality of the offending words exceed a certain threshold, that page is blocked (Khodaei, *et al*., 2011). Misspelling, over blocking of educational pages and text embedded in images makes this method unreliable for detection of adult content.

Visual features on the other hand provide more efficient feature for adult image identification (Arentz and Olstad, 2004; Wang *et al*., 1998) used a simple Bayesian classifier to detect skin regions in images. From these regions, they extracted texture features by employing Daubechies wavelets and used them for classification with image retrieval techniques. A maximum entropy model is built to detect skin pixels, in Lee *et al*. (2006) and elliptical features extracted from these regions are used for classification. In Shih *et al*. (2007), a learning-based chromatic-matching scheme is used for skin detection and features extracted from skin map of the image are incorporated for image classification by the Adaboost classifier. Won *et al*. (2002) used the HSV color space and MPEG-7 edge descriptors (Hammami *et al*., 2006; Hu *et al*., 2007; Ahmadi *et al*., 2010) to extract features from skin regions and classification is achieved using image retrieval techniques. In some objectionable image filtering systems, textual and visual features are combined together for image filtering (Kakumanu *et al*., 2007). These methods are mostly focused on the performance of the classifiers used for filtering purposes.

Skin detection is decisive step for objectionable image filtering. Skin detection can be divided into two categories: pixel-based and regional-based skin detection (Jones and Rehg, 2002; Kakumanu *et al*., 2007; Guerrero-Curieses *et al*., 2009; Nadian and Talebpour, 2011). Explicit rules, Bayes classifier, statistical models such as Gaussian distribution and GMM and Sinc function (Kaushal and Raina, 2010) are examples of pixel based methods where only pixel color information is considered for skin detection. Regional methods on the other hand incorporate

Corresponding Author: A. Nadian Ghomsheh, Department of Electronic and Computer Engineering, Shahid Beheshti University, GC, Tehran, Iran

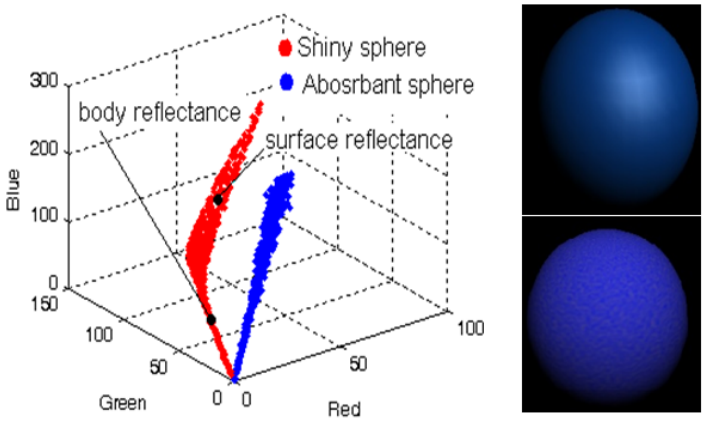

Fig. 1: Distribution of pixels in the RGB color space belonging to: (a) matte sphere and (b) shiny sphere

different techniques such as: Gabor wavelets (Fotouhi *et al*., 2009), Contour-lets (Wang *et al*., 2008), histogram matching (Störring *et al*., 2001; Ghomsheh *et al*., 2011) and physics based approaches (Shafer, 1985) to extract regional features for skin detection.

When skin is used as the primary step for adult image filtering two objectives are followed:

- Detecting images with none or small skin regions
- Distinguishing real skin regions from regions that have color similar to skin

In this regard, a two steps skin detection method is proposed which considers the two objectives. First, color information is used to detect images with no skin are small skin area with small computation overhead and then a regional method is incorporated to find the true skin regions among the remaining images. After extracting the final skin mask of the image, Area, texture, and the new shape feature are used for classifying images.

REVIEW OF DRM

A Color image is composed of three color components: red, green and blue (denoted accordingly with R, G and B for the rest of this study) and is obtained by:

$$C_i = \int_{\lambda} L(\lambda,\theta) s_i(\lambda) d\lambda \quad (1)$$

where, i∈ {R,G,B}, L(λ,θ) is the radiance spectrum, λ is the wavelength, θ is the photometric angle and s_i (λ) is the color filter transmission function. L(λ,θ), the amount of reflected light, is dependent on characteristics of the scene illuminant, the geometry of the object that reflects the light and the material that builds the object. These affecting parameters are explained by DRM, introduced by Shafer (Klinker *et al*., 1990):

$$L(\lambda,\theta) = L_s(\lambda,\theta_s) + L_b(\lambda,\theta_b) \quad (2)$$

L_s is the fraction of light that is directly reflected from the surface of an object (surface reflectance), and mostly resembles the color of the incident light source, since none of its components have been observed by the object (these are the specular points on the object). L_b which stands for body reflection, is the light that has penetrated into the object and then once again reflected from its surface, and corresponds to the actual color of the object (Fig. 1). Each term of Eq. 2 is dependent on spectral power distributions (C_s (λ) and C_b (λ)), geometric scaling factors (G_s (θ_s)) and $G_b(\theta_b)$), and coefficients of refraction (ρ_s and ρ_b). These parameters can be substituted into Eq. 2 which leads to:

$$C_i = G_S(i,n,v)\rho_S \int_{\lambda} c_S(\lambda) s_i(\lambda) d\lambda + G_b(i,n)\rho_b \int_{\lambda} c_b(\lambda) s_i(\lambda) d\lambda \quad (3)$$

The sensor sensitivities of a color camera are narrow band and can be approximated by delta function S_i (λ) = δ (λ - λ_i) (Shafer, 1985), therefore:

$$C_i = G_s(i,n,v)\rho_s c_s(\lambda_i) + G_b(i,n)\rho_b c_b(\lambda_i) \quad (4)$$

Under uniform lighting conditions Eq. 4 is simplified to:

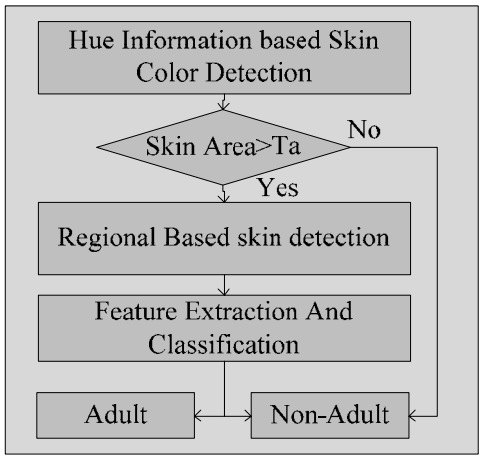

Fig. 2: Block diagram of the proposed algorithm

$$C_i = G_S(i,n,v)\rho_S \begin{bmatrix} C_{sR} \\ C_{sG} \\ C_{sB} \end{bmatrix} + G_b(i,n)\rho_b \begin{bmatrix} C_{bR} \\ C_{bG} \\ C_{bB} \end{bmatrix} \quad (5)$$

If an object reflects only the body component, the color of its pixels would distribute along a line in the direction of the color vector C_s times by constants G_s and ρ_s. If the surface reflectance is also present then this line at the boundary where L_s starts to appear, will bend towards the light source color (Fig .1). In both cases the pixels of an object will lie on plane in the RGB space (Störring *et al*., 2001). The following section describes how this behavior is utilized for detecting skin pixels.

PROPOSED SKIN DETECTION METHOD

Figure 2 shows the block diagram of the proposed method for adult image identification. The two steps of skin detection try to make a balance between accuracy and processing time required for detecting skin regions when considering adult image classification for large number of images. In the first step, using hue color information, an estimated skin mask of the image is obtained. This step is performed with high speed while preserving the accuracy of skin detection at a good rate. For images that have potential skin regions further processing is conducted. After each step of skin detection, images with none skin area, or small skin area are classified as normal images. For the remaining image, shape and texture feature are combined with area feature, and employed for image classification.

Skin detection using hue componen: Skin detection based on color information focuses on the distance of a color pixel to the skin color distribution. If this distance is closer than a predefined threshold, the corresponding pixel is classified as skin. Choosing a color space in which the skin color clusters in a smaller area of the space, results in a better classification of skin pixels. By reviewing DRM, it was explained how the pixels of an object distribute in the RGB color space. Figure 3a shows the distribution of skin pixels which belong to one skin sample. As it can be seen, these pixels span in a wide range, on each color component of the RGB color space.

Figure 3b shows the HSV is nonlinear color space and a cylindrical representation of the Cartesian RGB color space. Hue shows the dominant color of a region, Saturation is the amount of colorfulness of an area with respect to brightness and Value defines the color luminance. When skin pixels are transformed into the HSV color space, the projected values on the Hue component as can be seen in Fig. 3c span in a significantly smaller region of the Hue component. This is an expected behavior since the color of skin spans on a curve, in a plane (explained by DRM) and when projected on the Hue component, the projected area is a small interval on Hue. To this end, the Hue component is chosen for skin detection and consequently other than benefiting from smaller cluster, the dimensionality of the problem is reduced to one. HSV is transformed from RGB color space by:

$$H = \begin{cases} 0 & if \max = \min \\ \left(60^\circ \times \dfrac{G-B}{\max - \min}\right) \bmod 360^\circ & if \max = R \\ 60^\circ \times \dfrac{B-R}{\max - \min} + 120^\circ & if \max = G \\ 60^\circ \times \dfrac{R-G}{\max - \min} + 240^\circ & if \max = B \end{cases}$$

$$S = \begin{cases} 0 & if \max = 0 \\ 1 - (\min/\max) & otherwise \end{cases} \quad (6)$$

$$V = \max$$

where, max = max (R, G, B) and min = min (R, G, B). A test on ten million skin from 400 training images showed that for 99.5% of skin pixels R = max (R, G, B) holds true, and to speed the transformation process, (Eq. 6) is simplified into:

$$H = \begin{cases} 0 & if \ R = \min \\ \left(60^\circ \times \dfrac{G-B}{R - \min}\right) \bmod 360^\circ \end{cases} \quad (7)$$

Figure 3d shows the clustering of more than ten million skin pixels in the hue component, where skin pixels are ranged between $H_{low} = 0$ to $H_{high} = 50$. The algorithm used to extract skin pixels using color information as follows:

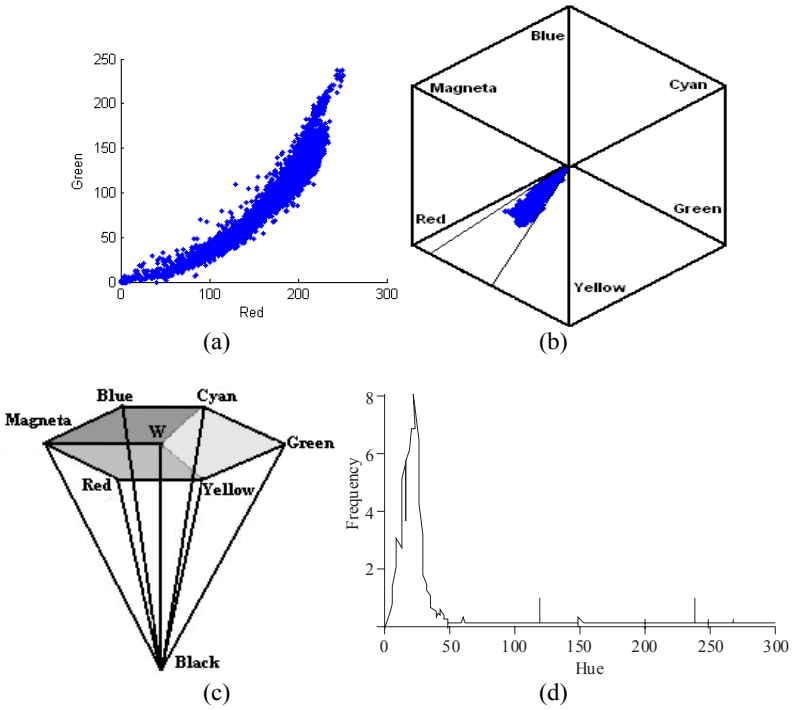

Fig. 3a: Skin distribution in R-G color space. (b) HSV color space and (c) skin color in HSV. (d) skin histogram on Hue.

- Convert RGB space to hue by (Eq. 7).
- Find the pixels with Hue values 10°<H<35°.
- Find the mean value (H_M) of H for pixels that are verified in step 2.
- Select pixels with $H\text{-}T_s<H_M<H+T_s$ as estimate of skin pixels in the image.

Steps (3) and (4) will let the skin detection process to be more dependent on the image data being processed. Therefore the hue range that is being detected as skin is limited between HM±Ts rather than the range H_{low} and H_{high}. Figure 4, top row shows two sample images where human skin and the background color are very similar. After performing step (3) and (4) the table has been eliminated and the correct skin region is extracted, the second image, the proposed method has failed to correctly exclude the back ground from the true skin region. Upon performing this step, the initial skin mask is extracted and images that were found to have large skin area are passed to next step for further inspection.

REGIONAL-BASED SKIN DETECTION

Human skin is found to have a surface reflectance of 5% (Chatterjee and Hadi, 2006); which indicates that, its color distribution deviates away from a straight line. Figure 5 shows the scattering of two different skin

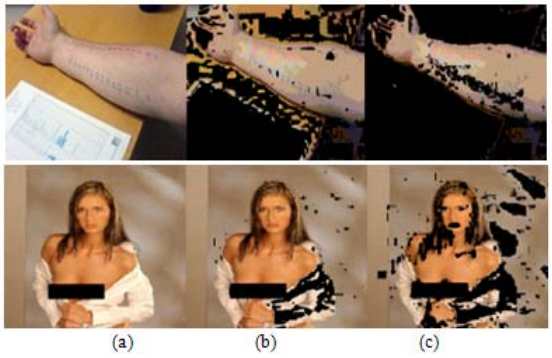

Fig. 4: Sample of Skin detection using color information

regions in the RGB color space. For each skin region, a small ribbon of the original skin is also shown. These samples show that skin distribution starts from the origin of the space and start to bend towards the white point.

To use this regional behavior of skin, an exponential function is used to be adapted to the histogram of skin pixels, projected into the R-G color plane. From the parameters of the fitted exponential it is decided if the selected region is human skin or not. The fitting function can be written as:

$$R(x, y) = 1 - e^{-(aG(x,y)+b)} \quad (8)$$

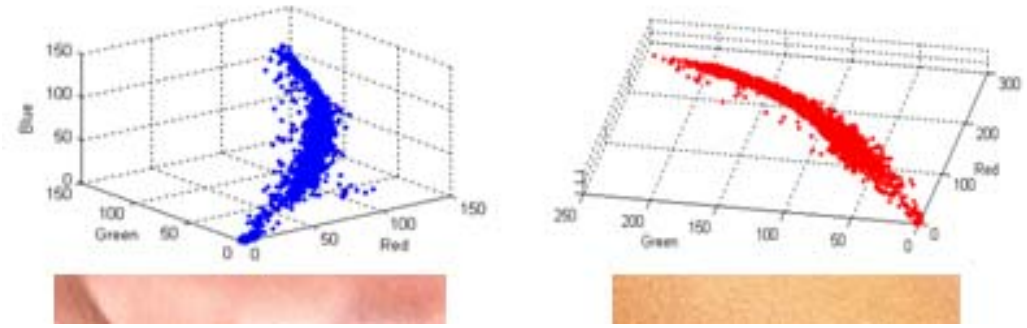

(a) (b)

Fig. 5: Two different skin samples and their color distribution in the RGB color space.

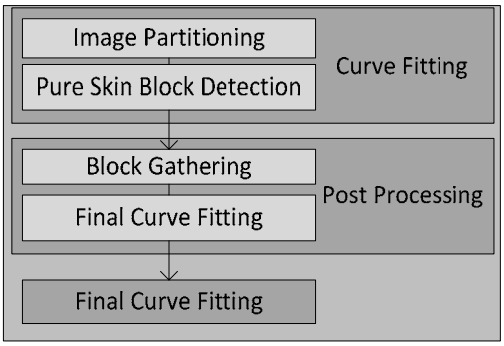

Fig. 6: Diagram of the regional-skin detection process

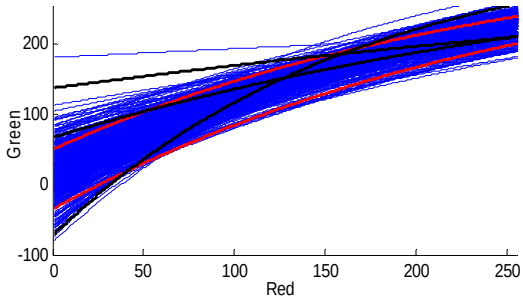

Fig. 7: The fitted exponential to the test image

where, a and b are the parameters that are tuned with respect to the histogram of estimated skin pixels from the previous step. This equation can be further simplified to take the form:

$$Ln(R-1) = -(aG + b) \quad (10)$$

where the problem can be simplified into a line fitting problem, where a and b are then easily calculated through the maximum likelihood estimation (Nadian and Talebpour, 2011). The histogram bin counts of skin pixels are used as the weighting parameter in the fitting process. Figure 6 shows different steps to extract the final skin mask using the regional method.

In this algorithm each image is first partitioned into 20×20 blocks and if more than 50% of the pixels are detected as skin, an exponential is fitted to the R-G histogram of that block. If the calculated a and b for the fitted function have values in the expected range, that block is considered as pure skin. To find the final skin region, all the pure skin blocks are merged together and using their information a new exponential that represent skin for that image is calculated. Pixels that are closer than threshold T to the exponential form the final skin mask.

To extract the ranges of a and b, 400 skin images are used as the training set. Figure 8 shows all the exponentials fitted to each image in the training set. The red lines in the image show the region for which if an exponential falls in, the corresponding block is considered as purse skin block. Doing so then a is found to be in interval [5.7 6], b is in [-1.2 -1.4] and T was set to 35. The black lines in Fig. 7 show many segments of exponentials that are not entirely in the range specified by the red lines, but still fall in the accepted region, thus enough skin blocks can be obtained to extract the final skin map of the image. Figure 8 shows the result of regional skin detection on the previously shown sample (Fig. 7). Figure 8a shows the image after first stage skin detection. The blocks detected as pure skin blocks are shown in Fig 9b and the final skin mask is shown in Fig 9c. The final exponential and detected skin pixels are shown in Fig. 9d.

FEATURE EXTRACTION AND CLASSIFICATION

After skin detection, the binary map of skin, I, is extracted, and from this map three features are extracted to describe the detected skin regions. Each feature is

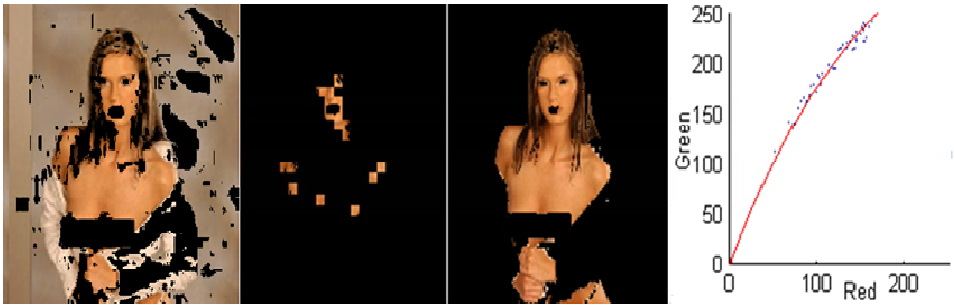

Fig. 8: Different steps of the regional skin detection method

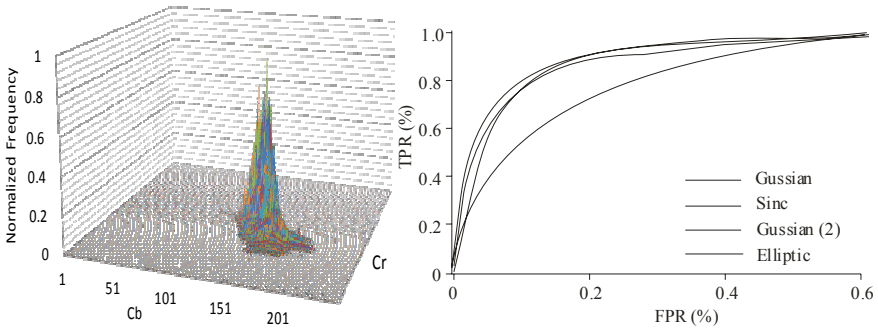

Fig. 9a: Histogram of skin pixels in Cb-Cr plane. (b) ROC curve analysis for parametric skin detection methods

explained as follows:

Area Feature (AF): Since most adult images have a large skin area, applying this feature is a very effective way to detect non-adult images with none or small skin area. The value of AF, which is defined as the ratio of total skin area to image area, is obtained through:

$$AF = \sum_{i=1}^{x,y} I(x,y) / A \quad (8)$$

where, A denotes the area of the binary image. By applying an area threshold, Ta, AF can be directly used to classify images with AF<Ta as normal images after skin detection, also area feature can be used along other features in the final classification phase.

Texture Feature (TF): Many objects with skin like color possess a different texture. Human skin is mostly a smooth area and thus no outstanding presentation of its texture can be found; therefore sophisticated and time consuming methods would not be very efficient. Here, Standard Deviation (StD) is used as a simple and fast method to calculate texture feature, which enables distinguishing between high and low textured skin regions. To extract TF, the gray skin map of the images is divided into non-overlapping windows with size Nt×Nt, and for each window, StD is calculated. TF is then described with a 32 bin resolution histogram calculated from StD values for all image blocks, and is arranged as:

$$TF = \{TF(1), TF(2), ..., TF(32)\} \quad (9)$$

Shape Feature (SF): To encode how the profile of the detected skin region resembles an adult image, SF is introduced. First, I is divided into W×W equal size blocks. For each block S(n) , if more than. 50% of pixels belong to the skin class, then S(n)=1, otherwise S(n)=0. The resulting $1 \times W^2$ vector that represents SF is arranged as:

$$SF = \{SF(1), SF(2), ..., SF(W^2)\} \quad (10)$$

In the classification phase, a Neural Network (NN) with one hidden layer is incorporated. The dataset used in this paper has 2400 images divided into two equal groups of adult and non-adult images, where 400 images from each class serve as the training data.

EXPERIMENTAL RESULTS

In the evaluation phase, each step of the proposed method is tested, and its result is compared with other state of the art methods. In this regard, first skin detection using color information, then regional skin detection step

Table 1: Skin detection using pixel color information

Method	Test case	TPR (%)	FPR (%)	Acc. (%)
Proposed	$T_s = 9°$	91.23	18.14	86.545
	$T_s = 10°$	93.21	19.46	86.875
	$T_s = 11°$	94.20	20.31	86.945
Gaussian	Case1	90.00	32.13	78.935
	Case2	95.00	47.95	73.525
GMM(2)	Case1	90.00	25.70	82.150
	Case2	95.00	42.40	76.300
Sinc	Case1	90.00	22.10	83.950
	Case2	95.00	40.620	77.190
Elliptic	Case1	90.00	45.57.5	72.215
	Case2	95.00	55.74	69.630

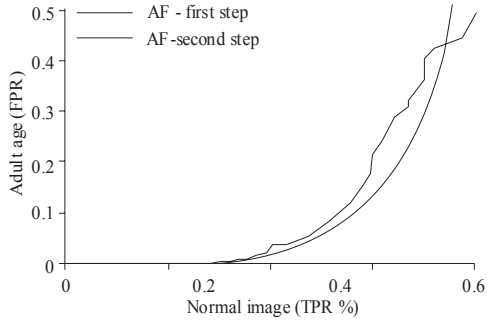

Fig. 10: Rate of filtering for TSR and LSR

and finally feature for adult image classification are tested.

Result of pixel based skin detection: To evaluate the performance of skin detection using Hue information, different parametric methods have been implemented and their performance is tested against the introduced skin detector. Gaussian distribution, GMM with 2 Gaussians, Elliptic boundary model and the Sinc function (Kakumanu *et al*., 2007), trained in the YCbCr color space are the implemented methods. YCbCr color space is chosen since it's known to be a better chrominance space for skin detection (Wang, *et al*., 1998). Figure 10a shows the skin color distribution in the Cb-Cr chrominance plane and Fig. 9b shows the ROC curves based on False Positive detection Rate (FPR) and True Positive detection Rate (TPR) for the implemented skin detection methods. From this figure, it can be seen that the mentioned methods do not yield high detection rates. Table 1 shows the result of first step skin detection using the proposed method for three values of T_s. For better comparison some numerical results obtained from Fig. 9b are also shown in the table.Case1 and Case2 are obtained by intersecting a horizontal line with the ROC curves so that TPR = 90 and 95%, respectively.

Results shown in this table indicate that the proposed method is superior in comparison to other pixel-based skin detection methods. For $T_s = 11^0$ the detected skin rate is near 95% where FPR for this threshold is 20.31%. This value is more than 20% percent better than the Sine model and 27% better than the Gaussian method. Based on accuracy, the proposed method is at least more than 9% more accurate for TPR = 95% when compared to other methods.

Table 2: Regional-based skin detection results

	TP (%)	FP (%)	Acc. (%)
Training set	96.10	4.3	95.90
Test set	95.02	6.2	94.41
Histogram matching	91.00	20.4	85.30
Adaptive model	95.20	17.4	88.90

Result of regional-based skin detection: After Skin detection using pixel color information, skin detection using the regional-based method is performed, where it is expected to eliminate a large amount of the false detected skin regions. The result of skin detection based on TPR and FPR for the test and train dataset are shown in Table 2. Also to evaluate the performance of the proposed methods, histogram matching (Dadgostar and Sarrafzadeh, 2006), and adaptive skin detection based on hue thresholding (Shih, *et al.*, 2007) methods are tested on the dataset.

According to the results shown in this table, in comparison to the result of first step skin detection, the overall skin detection rate was improved by 7.4% in accuracy. In comparison to other regional methods, tested on the data set, the propose method performed better with 9.1 and 5.5% compared to the histogram matching and adaptive skin detection methods.

Effect of applying T_a: To test the efficiency of *AF* as a crisp threshold to identify normal images in a pre-classification step, a threshold T_a is applied after skin detection. The ROC curve for adult image detection using T_a is shown after each step of the skin detection (Fig. 11). These ROC curves show that applying T_a is very efficient to correctly classify

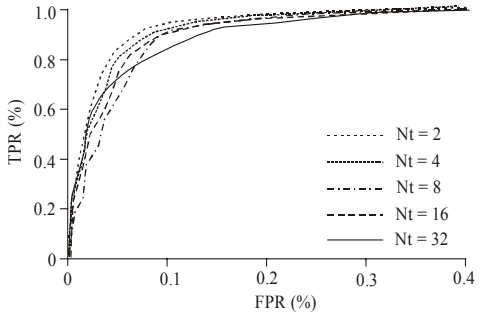

Fig. 11: Selecting N_t for TF

Table 3: Pre-detection of adult images using T_a

	AF, pixel-based (%)		AF, regional (%)	
TPR	T_a	TNR	T_a	TNR
99%	26	34.4	8	39.48
98%	30	38.9	12	41.48
95%	37	45.1	20	49.27

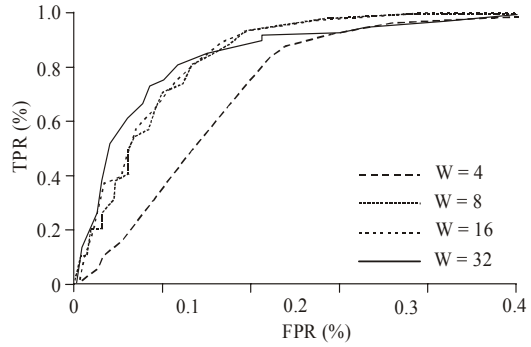

Fig. 12: Choosing W for shape feature

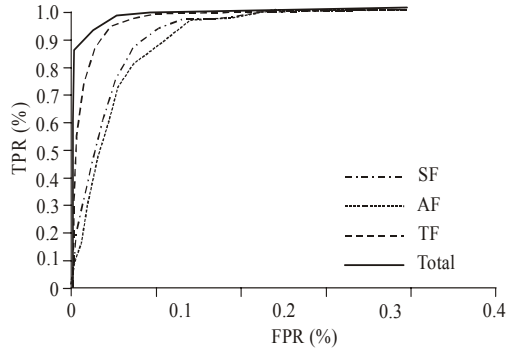

Fig. 13: Classification result on the test data set.

many normal images at a small cost in misclassification of adult images.

Table 3 shows the True Negative detection Rate (TNR) for fixed TPRs. For each TRP the corresponding T_a is also calculated from Fig. 10 and is shown in the table. It can be seen that for only 1% percent error acceptance on the adult image set it is possible to reject more than 30% of normal images from latter processing (in the test data set). As the error acceptance rate on adult images increases, the number of normal images that are correctly classified as skin is also increased. In this paper only 1% error on adult image classification rate is accepted and T_a = 26% is employed after first step skin detection.

Classification results: After detecting images with high skin area, the corresponding feature vector for each image is extracted. In order to find out the significance of each set of features: AF, TF, SF, and Total feature vectors are used to train a separate NN. The network that has been used in these experiments has one input, one hidden, and one output layer. In the training process each experiments is repeated ten times for different number of neurons in the hidden layer and the NN with best performance out of ten is selected for testing.

Texture and shape feature were formulated so that variable sized windows could be set for feature extraction. Figure 11 shows the result of classification using different window size for *TF* by changing N_t.

The result shown in the figure indicate that when $N_t = 2$ is chosen the best results is obtained. By increasing N_t up to 18, *TF* does not seem to be affected, but when $N_t = 32$ is chosen the classification rates start to degrade. The reason for this behavior is that when a large N_t is chosen, the diversity of data within a window increases and the *StD* is not an appropriate feature for distinguishing human skin from false skin-like regions. The overall result of this table shows that $N_t = 2$ was chosen for extracting texture feature.

To decide on size of *W*, this parameter is also test with several values and the result of classification is shown in Figure 12. These results show that when W = 8 and W = 16 are chosen, more convincing results are obtained, but for the other two cases the results are not very significant. This is an expected result since very large and very small windows cannot be a well representative of the shape feature. Because, big windows will not have enough information about the shape of an object and very small windows will also cause the problem of over fitting.

By selecting $W = 8$ and $N_t = 2$ a network including the *AF*, *TF* and *SF* is then trained to evaluate the classification rate when all feature are utilized. Figure 13 shows the classification result on the test data sets. Each trained NN that was chosen in the training process has been tested individually on

Table 4: Classification results based TPR and FPR

Feature	TPR(%)	FPR(%)	TPR (%)	FPR (%)
AF	90	22.75	95	26.75
SF	90	18.25	95	26.75
TF	90	6.75	95	13.25
Total	90	4.00	95	7.50

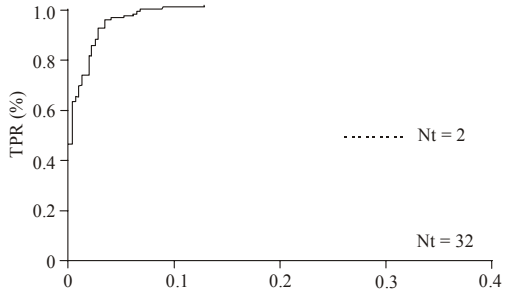

Fig. 14: Classification result with T_a=20%

Table 5: Classification result when Ta is applied

Ta>20% only		All images	
TPR	FPR	TPR	FPR
90	7.3	88.5	3
95	13.5	93.3	5.5

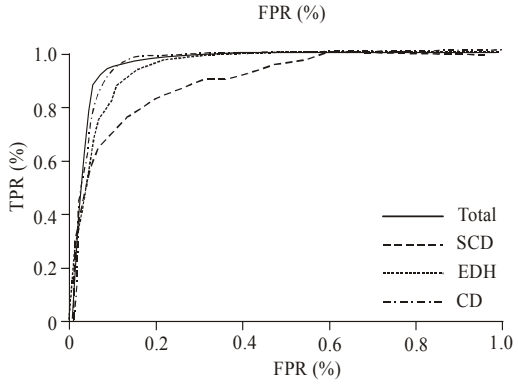

Fig. 15: Classification results using (Shih *et al*., 2007) feature (Lee *et al*., 2006).

the test data set. The results show that the combination of the features that were applied improved the overall classification rate. Table 4 summarizes some numerical values obtained from Fig. 13.

From the results shown in the table, it can be seen that for 90% TPR on adult images, only 4% of normal images have been classified as adult images. It can also be pointed out that the TF shows to be a very efficient feature and when used alone, only 6.75% error FPR has occurred on normal images. In this experiment, the feature extraction was conducted on all images and images with small or non-skin regions were not discarded in this process (T_s was applied). To see how the area feature can improve the performance of the system, an area threshold of 26% percent was employed after the first step of skin detection; where 1.7% of adult images and 59.25% percent of normal images were detected as normal images and were discarded in later steps. Figure 14 shows the output ROC curve of the NN output results for the remaining images. This figure shows that when, only images with large skin area are included for adult image classification, the features utilized in this process are well capable of distinguishing between adult and normal images. Table 5 shows the overall results; where the FPR in adult data set and TPR of normal image data set after employing T_a are combined with the results from Fig. 14.

This table shows that when T_a is applied, classification rate is improved by a small amount, but the number of images that have been classified as normal images after first step skin detection will greatly reduce the overall processing time required for detecting and classifying adult images.

For evaluating the significance of the proposed method; features presented in Lee *et al*. (2006) and Shih *et al*. (2007) are extracted for images in the data set experimented in this paper. These features include: Scalable Color Descriptor (SCD), Edge Oriented Histogram (EOH), from Lee *et al*. (2006) and Proportion of Skin Pixels (PSP), Location (LOC) and Shape feature from Shih *et al*. (2007).

Figure 15 shows that color does not provide significant information for classification, and hence poor claassification results are obtaind from color information. This is due to the fact that after skin detection, most skin detected regions posess the same properites and further color information does not significantly help improve the results. Shape and location feature in Fig. 16 did not yield high detection rates and the overall detection rate using location and shape features resulted in poor classification rate of adult and normal images.

For comparison between the proposed method and state of the art methods, Fig. 17. shows some numerical results based on the accuracy obtained from Fig. 13 trough 16. The first two cases are the results of the proposed method where Total shows the results when T_a is not applied after skin detection, and $Tatal+T_a$ is the case where T_a is applied after first step skin detection. using Total features, an accuracy of 93.9% is obtained while for the latter case the accuracy is found to be 93.75%. The accuracy of adult image identification using features

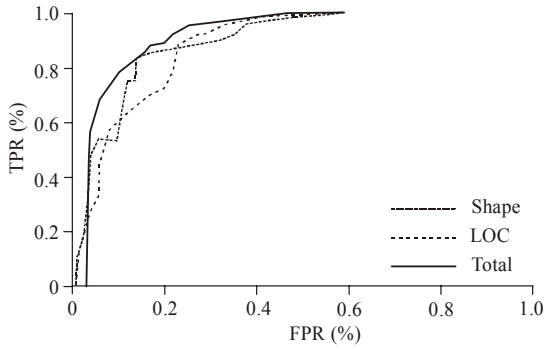

Fig. 16: Classification results using feature in Lee *et al*. (2006)

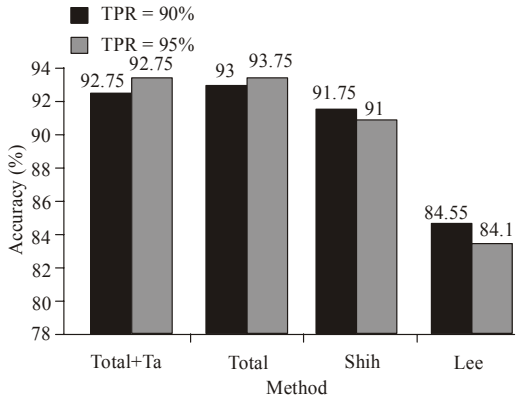

Fig.17: Comparison between accuracy of different feature sets on test images

proposed in Shih *et al*. (2007) is 84.55% for TPR = 90% and using features of an accuracy of 91.75% is yield. These results show that the poroposed features for classifying adult images is supirior to other state of the art methods.

CONCLUSION

In this study, an adult identification system using a new skin detection method was proposed. In the skin detection method, color pixel information using hue component of HSV color space were used to find an estimate skin map of the image. The accuracy of skin detection in this step was 86.87%, where compared to other pixel-based methods, at least 11% improvement was obtained. In the regional skin detection step by fitting an exponential to the histogram of the estimated skin region the final skin mask was extracted. By implementing this step with accuracy of 94.41%, result of first step skin detection was improved by more than 8%. Also the presented skin detector performed better than the histogram matching skin detection and the adaptive skin detection method by 9.11% and 5.5% respectively. The features extracted from the final skin mask were fed to a NN for classification of images as adult or normal images. Texture and the new shape feature proposed in this paper showed to be very efficient for adult image identification. The overall classification result with 93.9% accuracy showed that the proposed method was superior to other state of the art methods in the field of adult image classification which makes the proposed method highly applicable for adult image identification.

REFERENCES

Ahmadi, A., M. Fotouhi and M. Khaleghi, 2011. Intelligent classification of web pages using contextual and visual features. Appl. Soft. Comput., 11(2): 1638-1647.

Arentz, W.A. and B. Olstad, 2004. Classifying offensive sites based on image content. Comput. Vision Image Understand., 94(1-3): 295-310.

Chatterjee, S. and A.S. Hadi, 2006. Regression Analysis by Example. Wiley-Intersection, New Jersey.

D'Orlando, F., 2011. The demand for pornography. J. Happiness Stud., 12(1): 51-75.

Dadgostar, F. and A. Sarrafzadeh, 2006. An adaptive real-time skin detector based on hue thresholding: A comparison in two motion tracking methods. Pattern Recog. Lett., 27(12): 1342-1352.

Fotouhi, M., M.H. Rohban and S. Kasaei, 2009. Skin Detection using Contourlet-Based Texture Analysis. Computer Society of Iran Computer Conference, Tehran, pp: 59-64.

Ghomsheh, A.N., A. Talebpour and M. Basseri, 2011. Regional skin detection based on eliminating skin-like lambertian surfaces. IEEE Symposium on Computers and Informatics. Shahid Beheshti Univ., Tehran, Iran, pp: 307-312.

Guerrero-Curieses, A., J.L. Rojo-Álvarez, P. Conde-Pardo, J. Ramos-López, I. Landesa-Vázquez, *et al*., 2009. On the performance of kernel methods for skin color segmentation. Eurasip Journal on Advances in Signal Processing, 2009: Article no. 30, DOI: 10.1155/2009/856039.

Hammami, M., Y. Chahir and L. Chen, 2006. Webguard: A web filtering engine combining textual, structural and visual content-based analysis. IEEE T. Knowl. Data. Engin., 18(2): 272-284.

Haselton, B., 2007. Report on Accuracy Rate of FortiGuard Filter. Peacefire.org**,** Bellevue, WA, pp: 1-6.

Hu, W., O. Wu, Z. Chen, Z. Fu and S. Maybank, 2007. Recognition of pornographic web pages by classifying texts and images. IEEE T. Pattern Anal., 29(6): 1019-1034.

Jones, M.J. and J.M. Rehg, 2002. Statistical color models with application to skin detection. Int. J. Comput. Vision., 46(1): 81-96.

Kakumanu, P., S. Makrogiannis and N. Bourbakis 2007. A survey of skin-color modeling and detection methods. Pattern Recogn., 40(3): 1106-1122.

Kaushal, A. and J. Raina 2010. Face Detection using Neural Network and Gabor Wavelet Transform. Int. J. Comput. Sci. Tech., 1(1): 58-63.

Khodaei, A., C. Shahabi and C. Li, 2011. Hybrid indexing and seamless ranking of spatial and textual features of web documents. Lect. Notes. Comput. Sc., 6261: 450-466.

Klinker, G.J., S.A. Shafer and T. Kanade, 1990. A physical approach to color image undestanding.Int. J. Comput. Vision., 4(1): 7-38.

Kranich, N., 2004. Why filters won't protect children or adults. Lib. Admin. Manage., 18(1): 8-14.

Lee, J.S., Y.M. Kuo, P.C. Chung and E.L. Chen, 2006. Naked image detection based on adapitve and extensible skin color model. Patt. Recog., 40: 2261-2270.

Nadian, A. and A. Talebpour, 2011. Pixel-based skin detection using sinc function. IEEE Symposium on Computers and Informatics (ISCI), Dept. Electr. Comput. Eng., Shahid Beheshti Univ., Tehran, Iran, pp: 317-321.

Shafer, S.A., 1985. Using color to separate reflection components. Color Res. Appl., 10(4): 210.

Shih, J.L., C.H. Lee and C.S. Yang, 2007. An adult image identification system employing image retrieval technique. Pattern Recog. Lett., 28(16): 2367-2374.

Stol, W.P., H.K.W. Kaspersen, J. Kerstensa, E.R. Leukfeldta and A.R. Lodder, 2009. Governmental filtering of websites: The Dutch case. Comp. Law Secur. Rev., 25(3): 251-262.

Störring, M., H.J. Andersen and E. Granum, 2001. Physics based modelling of human skin colour under mixed illuminants. Robot. Auton. Syst., 35(3-4): 131-142.

Wai, H.H. and A.W. Paul 2004. Statistical and structural approaches to filtering internet pornography. IEEE Conference on Systems, Man and Cybernetics, Sudney.

Wang, J.Z., J. Li, G. Wiederhold and O. Firschein, 1998. System for screening objectionable images. Comp. Comm. J., 21(15): 1355-1360.

Wang, D., J. Ren, J. Jiang and S.I. Stan, 2008. Skin detection from different color spaces for model-based face detection. Comm. Com. Inf. Sc., 15(14): 487-494.

Won, C.S., D.K. Park and S.J. Park, 2002. Efficient use of MPEG-7 edge histogram descriptor. ETRI J., 24(1): 23-30.